

Research Article

Evaluation Of Absorbed Dose To Organs From ¹⁸F-FDG PET Imaging Using EGS5 Monte Carlo Simulations.

Shlomi Caduri^{1,2} and Itzhak Orion¹.

1. Department of Nuclear Engineering, Ben-Gurion University of the Negev, POB 653, Beer-Sheva 84105, Israel.
2. Schneider Children's Medical Center, Kaplan St 14, POB 559, Petah Tikva, Israel, and Rabin Medical Center 39, Jabotinsky St., Petah Tikva 49100, Israel.

Abstract

The accurate evaluation of doses absorbed by organs during ¹⁸F-FDG PET scans is a critical issue in operational radiological protection and thus requires the application of the most accurate calculation approaches available. Radiation transport using the Monte Carlo method is the gold standard in medical physics for calculations of dose distributions in complex structures. Recently, positron source Monte Carlo simulation results were compared to measurements and found to be in a good agreement.

The current study aims to use EGS5 Monte Carlo simulations to accurately estimate the ¹⁸F-FDG absorbed dose to the kidney and to the red bone marrow of the upper arm. The dose obtained from the simulations will be compared to dose values published in reports by the International Commission on Radiological Protection (ICRP).

The percentage difference in doses between the Monte Carlo results for the ICRP 106 and ICRP 53 in adult kidneys ranged from 2% to 21%. The absorbed dose Monte Carlo results for arm red bone marrow in children, due to ¹⁸FDG injection, were found to be higher by about 2.35%. That dose should be added to the previously estimated total red bone marrow dose. The findings of the present study demonstrate that the estimation of organ absorbed dose based on ICRP dose coefficient involving administration of the ¹⁸F-FDG substance is significant for future research, especially regarding radiation protection areas, because it affects the calculation of organ absorbed dose.

Keywords : PET, radiation, dose, positron, imaging.

INTRODUCTION

Patient safety is of great significance in treatments involving ionizing radiation. The amount of total radiation exposure from medical treatments or diagnostics has continuously risen from the early 1980s to the present day¹. In 2008, the estimated number of diagnostic and interventional radiological procedures (including dental) carried out annually worldwide was 3.6 billion, while the estimated number of nuclear medicine procedures was over 30 million, and the estimated number of radiation therapy procedures was over 5 million². The number of such procedures has continued to rise since then. These medical radiation methods offer significant public health benefits. However, ionizing radiation is hazardous and can cause damage. A systematic approach should be applied to guarantee a balance between obtaining

the benefits offered by the medical utilization of ionizing radiation and reducing the risk of radiation effects to patients, workers, and the general population.

Positron emission tomography (PET) plays an increasingly important role in medical diagnostics, particularly in nuclear imaging. PET is commonly used in the diagnosis of cancer, frequently to characterize general metabolic activities. FDG PET has proven to be a sensitive imaging modality for detection, staging and restaging, and therapy response assessment in oncology^{3,4,5,6,7,8,9,10,11,12,10}. FDG PET/CT also plays an increasingly relevant role in inflammation and infection imaging¹³.

A PET scan involves injecting a positron-emitting radioactive isotope into the body; this is usually complexed to a "carrier" molecule that confers biological specificity. The most frequently used radioisotope is Fluorine-18, which

***Corresponding Author:** Prof. Itzhak Orion, Department of Nuclear Engineering, Ben-Gurion University of the Negev, POB 653, Beer-Sheva 84105, Israel.

E-mail: iorion@bgu.ac.il

Received: 19-Jan-2025, Manuscript No. WJMOY-4465 ; **Editor Assigned:** 25-Jan-2025 ; **Reviewed:** 11-Feb-2025, QC No. WJMOY-4465 ; **Published:** 14-Feb-2025, DOI: 10.52338/wjciongy.2025.4465

Citation: S. Caduri and I. Orion. Evaluation of Absorbed Dose to Organs From ¹⁸F-FDG PET Imaging using EGS5 Monte Carlo Simulations. World Journal of Medical Oncology. 2025 January; 9(1). doi: 10.52338/wjciongy.2025.4465.

Copyright © 2025 Prof. Itzhak Orion. This is an open access article distributed under the Creative Commons Attribution License, which permits unrestricted use, distribution, and reproduction in any medium, provided the original work is properly cited.

combines with glucose to form a radiopharmaceutical named flourodeoxyglucose (FDG). The FDG is trapped by cells that consume high amounts of glucose, thereby attracting the positron emitter to sites of high metabolic activity (e.g., a tumor). Positrons are emitted at these sites with quite high initial kinetic energy (~300 keV), and they must slow down or thermalize in the body to energies less than 100 eV before they can pick up an electron by forming Positronium (Ps), or track a free electron, and then annihilate to produce two correlated photons¹⁴. These photons are then imaged using high-resolution, sensitive radiation detectors. Computer algorithms to form 3-D images can recognize tumors with high precision, enabling diagnosis, treatment planning, and treatment monitoring. As mentioned, the most commonly used PET radiotracer is the glucose analog 2-[18F] fluoro-2-deoxy-d-glucose (18F-FDG). A typical clinical scan involving the administration of 350-750 MBq of 18F-FDG 15 exposes most tissues in an average patient to a maximum absorbed dose of approximately 10 mGy from positron emission (β^+ , $E_{max} = 634$ keV) and annihilation photons (γ -rays, 511 keV). However, tissues with increased uptake of the radiopharmaceutical receive higher absorbed doses than the whole-body average, including the brain (10–36 mGy), heart (16–51 mGy), kidneys (7–23 mGy), and bladder (13–233 mGy)^{16,17,18,19,20}.

Absorbed doses in organs can be used to compare radiation exposure among medical imaging procedures, to compare options regarding alternative imaging methods, and to guide dose optimization efforts. Individual organ dose estimates are important for relatively radiosensitive patient populations, such as children, and for radiosensitive organs. In this study, the organ absorbed dose per injected activity (AD/IA) was calculated for adult kidneys and for pediatric arm red bone marrow for the radiopharmaceutical 18F-FDG using Monte Carlo (MC) methods. We chose to focus on these two organs due to their vulnerability to ionizing radiation. The kidney is known to be a highly radiosensitive organ due to high uptake and retention of the radionuclides after glomerular filtration²¹. The second organ evaluated in this paper, pediatric arm red bone marrow, was chosen due to its high exposure when performing intravenous injection of 18F-FDG. Apart from that, the red bone marrow is known to be highly radiosensitive because it has large molecules, such as intact antibodies with very slow kinetic rates, which circulate in the bloodstream for an extended period. Therefore, the radiation from decaying radionuclides may contribute considerably to dose absorbed by the blood-rich red marrow²².

METHODS

Several Monte Carlo code systems include positron transport and can model dosimetry for positron applications. The Monte Carlo method is based on computerized pseudo-random

numbers to sample probability distributions governing the physical processes involved. The radiation transport in general and positron transport in particular are good phenomena for evaluation by the Monte Carlo method. In radiation transport, electron, positron, and photon showers are simulated by compiling many repetitions of physical processes that follow probability distributions.

As our previous study demonstrated, using the EGS5 code system for internal positron dose evaluations was found preferable to using GAMOS (the Geant4-based Architecture for Medicine-Oriented Simulations)²³.

The EGS5 code is the upgraded version of the fourth version of EGS (Electron Gamma Shower) code²⁴. In EGS5 code, the new transport mechanism is based on the dual hinge methodology that performs an electron or a positron scattering hinge treated by randomly split sub-steps. Full details of the electron or positron transport scheme were published by Wilderman et al.^{25,26}.

A. Kidney model

Biokinetic model for kidneys

The F-18 has a physical half-life of 1.83 hours. However, it is necessary to consider its biological half-life as well. The activity curves as functions of time in the kidneys were built using the available F-18 biokinetic data from ICRP Publications 53⁽²⁷⁾ and 128⁽²⁸⁾ and ICRP Publication 106⁽²⁹⁾. Assuming immediate uptake of the administered activity A_0 , the activity as a function of time $A_s(t)$ in the source organ S with an effective half-life $T_{i,eff}$ can be expressed as:

$$\frac{A_s(t)}{A_0} = F_s \sum_{i=0}^n a_i e^{\left(\frac{-\ln 2}{T_{i,eff}} t\right)} \quad (1)$$

Where F_s is the fraction of the administered radiopharmaceutical incorporated by the organ S; a_i is the fraction of F_s eliminated with a biological half-life T_i ; and n is the number of elimination components. The effective half-life, $T_{i,eff}$ is given by Equation 2, where T_i and T_p are the biological and physical half-life, respectively:

$$\frac{1}{T_{i,eff}} = \frac{1}{T_i} + \frac{1}{T_p} \quad (2)$$

The cumulated activity, \tilde{A}_s , is given by Equation 3, which is the quantity used to determine the absorbed dose, by making use of the ICRP dose coefficients.

$$\frac{A_s}{A_0} = F_s \sum_{i=0}^n a_i \frac{T_{i,eff}}{\ln 2} e^{\left(\frac{-\ln 2}{T_{i,eff}} t\right)} \quad (3)$$

Table 1 presents the F_s factor for several organs taken from ICRP 106²⁹. As can be seen, there is an initial uptake of 18F-FDG in heart (0.04), brain (0.08), liver (0.05), lungs (0.03), and all other tissues (0.8). The retention in the specified source organs is considered to be infinite (without consideration of a delayed uptake). A fraction of 0.3 of the activity in other

organs and tissues is considered to be excreted in urine with biological half-times of 12 min (25%) and 1.5 h (75%), according to the kidney–bladder model. This model assumes that the fraction of the total excretion which passes through the kidneys and bladder is known. Activity excreted via this route passes through the kidneys with a transit time established from other clinical studies, subsequently entering the bladder in the urine and remaining there until the bladder is emptied and the radioactive contents leave the body.

Table 1. Biokinetic data for 18F-FDG from ICRP 106²⁹.

Organ (S)	Fs
Brain	0.08
Heart wall	0.04
Lungs	0.03
Liver	0.05
Other organs and tissues	0.8
Urinary bladder contents	0.24

Regarding the ICRP methodology, the cumulated absorbed dose in kidneys is estimated by multiplying the administered activity by the corresponding given dose coefficients.

The absorbed dose per injected activity calculated by Monte Carlo simulation in this study was compared with the data available in the ICRP 53²⁷ and ICRP 106²⁹. The recommended dose coefficients for 18FDG described in Table 2 were multiplied by administered activity of 370 MBq^{15,30}. **Table 2** summarizes dose calculations for kidneys performed both from ICRP 106²⁹ and from ICRP 53²⁷ for adults and 15-, 10-, 5-, and 1-year-old children.

Table 2. Absorbed doses for 18F-FDG based on the reports ICRP 106²⁹ and ICRP 53²⁷.

Kidneys	Administered absorbed dose per activity (mGy/MBq)				
	Adult	15 years	10 years	5 years	1 year
ICRP 106 (and 128)	1.7E-02	2.1E-02	2.9E-02	4.5E-02	7.8E-02
ICRP 53 (and 80)	2.1E-02	2.5E-02	3.6E-02	5.3E-02	9.4E-02

The difference in dose between ICRP 106²⁹ and ICRP 53²⁷ ranges from 17.7% up to 24%. ICRP 53²⁷ is always higher and 23% more in adults.

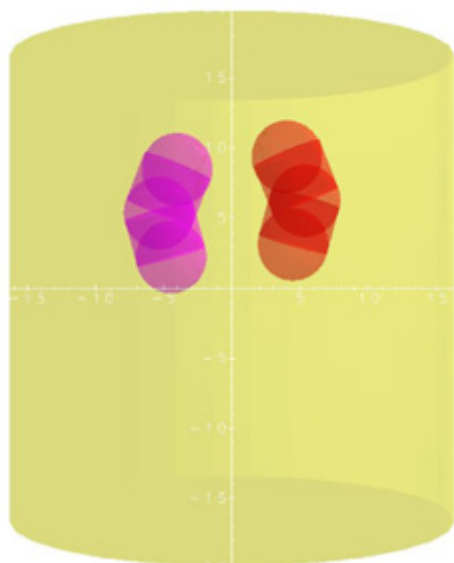
Kidney simulation setup

All simulations were conducted using the EGS5 Monte Carlo code system with 10 million histories (repeats) each. The simulation included the geometry, the materials, and positron source descriptions with the following details. A kidney is represented by three combined spheres connected by two cylinders with a radius of 2.9 cm. The kidneys were placed inside a cylindrical volume representing the abdomen. Each kidney has a volume of 299 cm³ (approximate to the volume in the ICRP 110³¹ for a male kidney, which is 295 cm³). The left kidney was placed 1 cm higher than the right one due to anatomical structure, as shown in **Fig. 1**. The dimensions used to create the kidney model are shown in **Table 3**.

Table 3. Dimensions for the kidney (based on ICRP 89³²).

Dimensions	Adults (cm)
Length	10-12
Transverse diameter	5-6
Anteroposterior diameter	3-4
Width	
Cortex	0.8(0.4-1.3)
Medulla	1.6-1.9
Thickness of capsule	0.01 -0.02

Figure 1. The kidneys MC model as defined in the EGS5 simulations



The elemental composition parameters of the kidney based on ICRP Publication 110³¹ were: H =10.3, C= 12.4, N=3.0, O=73.1, Na=0.2, P=0.2, S=0.2, Cl=0.2, K=0.2, Ca=0.1 (percentage by weight), with mass density of 1.05 [g/cm³] .

The elemental composition parameters of the abdomen (muscle) are: H =10.2, C= 14.3, N=3.4, O=71.0, Na=0.1, P=0.2, S=0.3, Cl=0.1, K=0.4 (percentage by weight), with mass density of 1.05 [g/cm³].

We performed the simulations under two irradiation conditions: one for the right kidney and one for the left. Each positron source was homogeneously placed inside the middle sphere of the kidney and emitted in a random direction and with an energy sampled from the F-18 energy spectrum.

To generate uniformly distributed points inside a sphere, we generated a real number over a uniform random variable $U(0,1)$ for r, θ, φ with the following distribution and converted it into a random point in x, y, z inside the sphere:

$$\begin{aligned} r &= R \times (U(0,1))^{\frac{1}{3}}, \\ \theta &= \arccos(1-2U(0,1)), \\ \varphi &= 2\pi U(0,1), \\ x &= r \sin(\theta) \cos(\varphi), \quad y = r \sin(\theta) \sin(\varphi), \quad z = r \cos(\theta) \end{aligned}$$

To generate isotropic distribution of direction we again generated θ, φ as mentioned above and used the following direction:

$$\mathbf{u} = \sin(\theta) \cos(\varphi), \quad \mathbf{v} = \sin(\theta) \sin(\varphi), \quad \mathbf{w} = \cos(\theta)$$

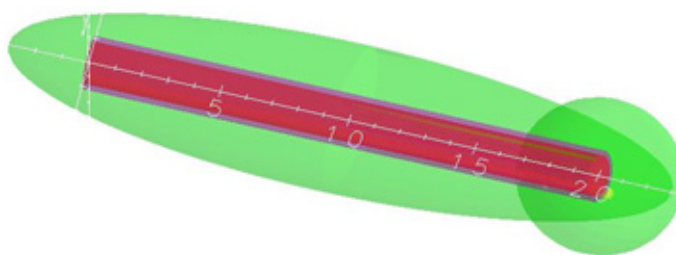
10^7 positron histories were generated and uniformly distributed throughout the kidney volume. This number of histories leads to a 0.2% statistical error in the kidney zone.

B. Arm model

Pediatric arm simulation setup

When performing the intravenous injection of ¹⁸F-FDG, the red bone marrow in the upper arm mostly receives radiation exposure. The pediatric arm model was optimized to reflect a five-year-old pediatric upper arm. In this current model, the arm has a cylindrical tube, representing the humerus bone with a diameter of 20 mm, and bone marrow inside it with an internal diameter of 16 mm. The bone was placed inside an ellipsoid with a sphere on the top of it, representing the muscles of the arm. A cylindrical tube with a diameter of 4 mm, filled with blood, was placed next to the bone, representing the Basilic vein, as evinced in **Fig. 2**. Each positron source was homogeneously placed inside the vein and emitted in a random direction and with an energy sampled from the F18 energy spectrum.

Figure 2. Pediatric arm MC model as defined in the EGS5 simulations.



To generate uniformly distributed points inside the vein, we generated uniform distribution on a disk (y coordinate and R is the radius of the vein) along the entire height of the vein (h):

$$\begin{aligned} r &= R \times U(0,1), \\ \theta &= \arccos(1-2U(0,1)), \\ \varphi &= 2\pi U(0,1), \\ x &= r \cos(\theta), \quad y = r \sin(\theta), \quad z = h U(0,1) \end{aligned}$$

The radiation direction was isotropically distributed.

10^7 positron histories were generated and uniformly distributed throughout the arm.

The elemental composition data was taken from ICRP Publication 70³³, and the anatomical data was taken from³⁴.

Table 4. The elemental composition parameters (percentage by weight) and their mass density used for the arm structure

	H	C	N	O	Na	Mg	P	S	Cl	K	Ca	Fe	Density [g/cm ³]
Red bone marrow	10.5	41.5	4.1	43.9	0.1	0.2	0.2	0.2	-	-	-	0.1	1.03
Bone	4	16	4.5	46.9	0.1	0.2	9	0.3	-	-	1.9	-	1.66
Blood	10.2	11	3.3	74.5	0.1	-	0.1	0.2	0.3	0.2	-	0.1	1.06
Muscle	10.2	14.3	3.4	71	0.1	-	0.2	0.3	0.1	0.4	-	-	1.05

RESULTS AND DISCUSSION

Kidney Simulation using EGS5

The results of EGS5 simulations for absorbed dose per event are shown in **Table 5**. The difference in the statistical error can be explained by the fact that in a given simulation one kidney consists of the positron source, while the second kidney is passive and receives its absorbed dose from the far kidney, and vice versa.

Table 5. Absorbed dose for kidneys. The simulations were performed under two irradiation conditions: one for the right kidney and one for the left. The volume of the right and the left kidney in both cases is identical. The mean energy values represent the relative part of the total of energy deposition for each kidney.

Source	Region	Mean Energy per event (%)	Absorbed Dose (Grey per incidence)	Statistical error
Left kidney	Left kidney	2.79E-01	3.56E-14	0.02%
	Right Kidney	4.03E-03	5.14E-16	0.2%
Right Kidney	Left kidney	3.98E-03	5.08E-16	0.2%
	Right kidney	2.79E-01	3.56E-14	0.02%

The absorbed dose according to the ICRP was calculated using the adults' values from Table 2, obtained 1.7E-02 mGy/MBq (ICRP106²⁹) and 2.1E-02 mGy/MBq (ICRP53²⁷) and multiplied by the administered activity of 370 MBq. The absorbed dose according to the Monte Carlo simulation results was calculated using $\frac{\bar{A}}{A_0} = 0.13$ for one kidney multiplied by the EGS5 results and the administered activity of 370 MBq.

The percentage difference between ICRP calculated dose and the EGS5 calculated dose was calculated using the following equation:

$$\text{Difference \%} = \frac{\text{ICRP calculated (mGy)} - \text{EGS5 calculated (mGy)}}{\text{ICRP calculated (mGy)}} \times 100$$

As shown in **Table 6**, the percentage difference between our results and the ICRP 106²⁹ and ICRP 53²⁷ in adult kidney doses ranged from 2% to 21%.

Table 6. Comparison of absorbed dose for kidney. The absorbed dose according to the ICRP was calculated using the adults' values from Table 2.

	Dose in kidney (mGy)	Difference (%)
ICRP 106	6.29	2%
ICRP 53	7.77	21%
EGS5	6.16 ± 0.06	

Pediatric arm simulation using EGS5

The results of EGS5 simulations for absorbed dose per event are shown in **Table 7**.

Table 7. Absorbed dose for pediatric arm. The pediatric arm model was optimized to reflect a five-year-old pediatric upper arm. The mean energy values represent the relative part of the total energy deposition for each part.

Region	Volume (cm ³)	Mean Energy per event	Absorbed Dose (Grey per event)	Statistical error
Red bone marrow	40.2	9.01E-03	8.71E-15	0.4%
Bone	22.6	8.87E-03	9.45E-15	0.4%
Blood	2.52	1.82E-01	2.73E-12	0.02%
Muscle	335	6.18E-02	7.02E-15	0.1%

The absorbed dose according to the ICRP was calculated using five-year-old values from ICRP106²⁹ and ICRP53²⁷, which in this case both have the same value of 3.2E-02 mGy/MBq, and multiplied by administered activity of 111 MBq (average weight of 20 kg and administered activity of 0.15 mCi per kg). Following intravenous administration, most of the FDG clears rapidly from the circulation with a half-time of less than 1 min because it mixes within a large distribution space (ICRP 106²⁹); hence, the absorbed dose to the red bone marrow was calculated using $\frac{A_s}{A_0}$ (sec)=86.4 multiplied using administered activity of 222 MBq and with the EGS5 results. The total absorbed dose given to the red bone marrow until final excretion of the FDG from the body is 3.552 mGy. The absorbed dose to the upper arm red bone marrow during the injection is 0.0835 mGy, which is 2.35%.

CONCLUSIONS

This study aimed to describe a novel approach for modelling the absorbed dose during 18FDG injection. Considering the increasing frequency with which whole-body PET/CT examinations are conducted, detailed assessments of the 18FDG dose are important; indeed, they directly expose radiosensitive organs. In this study we found that there is good agreement in estimated organ doses for kidneys between ICRP 106²⁹ dose coefficient and our results. The percentage doses difference between our results and the ICRP 106²⁹ in adult kidneys ranged from 2% to 21%. Hence, the findings in the present study demonstrated that the estimation of organ absorbed dose based on ICRP dose coefficient involving administration of the 18FDG substance is significant for future research, especially regarding radiation protection area, because it affects the calculation of organ absorbed dose. For comparison, the effective dose (radiopharmaceutical organ dose is estimated utilizing conversion coefficients and injected activity and CT organ dose utilizing tissue-weighting factors³⁵), according to our calculation is 6.16 mSv for the kidney while a kidney dose with low dose non-contrast CT for evaluation of patients suspected of suffering from stone disease is 3 mSv³⁶. A diagnostic quality CT average whole body scan effective dose is 15mSv³⁷, and the global average background radiation is 2.4 mSv per year reported by UNSCEAR³⁸. The absorbed dose in arm red bone marrow in children due to 18FDG

injection obtains a higher dose of about 2.35% that should be added to the previously estimated total red bone marrow dose.

Acknowledgements

We thank Dr. Rebecca Wolpe for the language editing of this manuscript.

REFERENCES

- Schauer DA, Linton OW. National Council on Radiation Protection and Measurements report shows substantial medical exposure increase. *Radiology*. 2009;253(2):293-296. doi:10.1148/radiol.2532090494
- Radiation Protection and Safety in Medical Uses of Ionizing Radiation. Vienna: INTERNATIONAL ATOMIC ENERGY AGENCY; 2018. <https://www.iaea.org/publications/11102/radiation-protection-and-safety-in-medical-uses-of-ionizing-radiation>.
- Avril NE, Weber WA. Monitoring response to treatment in patients utilizing PET. *Radiol Clin North Am*. 2005;43(1):189-204. doi:10.1016/j.rcl.2004.09.006
- Bastiaannet E, Groen H, Jager PL, et al. The value of FDG-PET in the detection, grading and response to therapy of soft tissue and bone sarcomas; a systematic review and meta-analysis. *Cancer Treat Rev*. 2004;30(1):83-101. doi:10.1016/j.ctrv.2003.07.004
- Borst GR, Belderbos JSA, Boellaard R, et al. Standardised FDG uptake: A prognostic factor for inoperable non-small cell lung cancer. *Eur J Cancer*. 2005;41(11):1533-1541. doi:10.1016/j.ejca.2005.03.026
- de Geus-Oei L-F, van der Heijden HFM, Corstens FHM, Oyen WJG. Predictive and prognostic value of FDG-PET in nonsmall-cell lung cancer. *Cancer*. 2007;110(8):1654-1664. doi:10.1002/cncr.22979
- Hoekstra CJ, Stroobants SG, Smit EF, et al. Prognostic Relevance of Response Evaluation Using [¹⁸F]-2-Fluoro-

- 2-Deoxy-D-Glucose Positron Emission Tomography in Patients With Locally Advanced Non-Small-Cell Lung Cancer. *J Clin Oncol.* 2005;23(33):8362-8370. doi:10.1200/JCO.2005.01.1189
8. Vansteenkiste JF, Stroobants SG. The role of positron emission tomography with 18F-fluoro-2-deoxy-D-glucose in respiratory oncology. *Eur Respir J.* 2001;17(4):802-820. doi:10.1183/09031936.01.17408020
 9. Weber WA. Use of PET for monitoring cancer therapy and for predicting outcome. *J Nucl Med.* 2005;46(6):983-995.
 10. Fletcher JW, Djulbegovic B, Soares HP, et al. Recommendations on the use of 18F-FDG PET in oncology. *J Nucl Med.* 2008;49(3):480-508. doi:10.2967/JNUMED.107.047787
 11. Delgado-Bolton R, Carreras J, Perez-Castejon M. A Systematic Review of the Efficacy of 18F-FDG PET in Unknown Primary Tumors. *Curr Med Imaging Rev.* 2006;2(2):215-225. doi:10.2174/157340506776930601
 12. Delgado-Bolton RC, Fernández-Pérez C, González-Maté A, Carreras JL. Meta-analysis of the performance of 18F-FDG PET in primary tumor detection in unknown primary tumors. *J Nucl Med.* 2003;44(8):1301-1314.
 13. Jamar F, Buscombe J, Chiti A, et al. EANM/SNMMI guideline for 18F-FDG use in inflammation and infection. *J Nucl Med.* 2013;54(4):647-658. doi:10.2967/JNUMED.112.112524
 14. Garcia G, Lj Petrović Z, White R, Buckman S. Monte Carlo model of positron transport in water: Track structures based on atomic and molecular scattering data for positrons. *IEEE Trans Plasma Sci.* 2011;39(11 PART 1):2962-2963. doi:10.1109/TPS.2011.2166790
 15. Schelbert HR, Hoh CK, Royal HD, et al. Procedure guideline for tumor imaging using fluorine-18-FDG. Society of Nuclear Medicine. *J Nucl Med.* 1998;39(7):1302-1305.
 16. Deloar HM, Fujiwara T, Shidahara M, et al. Estimation of absorbed dose for 2-[F-18]fluoro-2-deoxy-D-glucose using whole-body positron emission tomography and magnetic resonance imaging. *Eur J Nucl Med.* 1998;25(6):565-574. doi:10.1007/s002590050257
 17. Deloar HM, Fujiwara T, Shidahara M, Nakamura T, Yamadera A, Itoh M. Internal absorbed dose estimation by a TLD method for 18F-FDG and comparison with the dose estimates from whole body PET. *Phys Med Biol.* 1999;44(2):595-606. doi:10.1088/0031-9155/44/2/021
 18. Brix G, Lechel U, Glatting G, et al. Radiation exposure of patients undergoing whole-body dual-modality 18F-FDG PET/CT examinations. *J Nucl Med.* 2005;46(4):608-613.
 19. Mejia AA, Nakamura T, Masatoshi I, Hatazawa J, Masaki M, Watanuki S. Estimation of absorbed doses in humans due to intravenous administration of fluorine-18-fluorodeoxyglucose in PET studies. *J Nucl Med.* 1991;32(4):699-706.
 20. Hays MT, Watson EE, Thomas SR, Stabin M. MIRD Dose Estimate Report No. 19: Radiation Absorbed Dose Estimates from 18 F-FDG. *J Nucl Med.* 2002;43:210-214.
 21. De Jong M, Valkema R, Van Gameren A, et al. Inhomogeneous localization of radioactivity in the human kidney after injection of [(111)In-DTPA] octreotide. *J Nucl Med.* 2004;45(7):1168-1171. <http://www.ncbi.nlm.nih.gov/pubmed/15235063>.
 22. Larsson E, Ljungberg M, Mårtensson L, et al. Use of Monte Carlo simulations with a realistic rat phantom for examining the correlation between hematopoietic system response and red marrow absorbed dose in Brown Norway rats undergoing radionuclide therapy with 177 Lu- and 90 Y-BR96 mAbs. *Med Phys.* 2012;39(7Part1):4434-4443. doi:10.1118/1.4730499
 23. Caduri S, Lantsberg S, Bassevitz RF, Orion I. Dosimetry of positrons from PET radiotracers using Monte Carlo simulations and measurements. *Radiat Phys Chem.* 2023;207:110865. doi:10.1016/J.RADPHYSHEM.2023.110865
 24. Hirayama H, Namito Y, Bielajew AF, Wilderman SJ, R. NW. The EGS5 Code System. SLAC-R-730, ; 2005. doi:10.1177/016235329401800105
 25. Wilderman SJ, Bielajew AF. Modified random hinge transport mechanics and multiple scattering step-size selection in EGS5. 2005. https://inis.iaea.org/search/search.aspx?orig_q=RN:38043955. Accessed March 16, 2023.
 26. Wilderman S. Automated Electron Step Size Optimization in Egs5. Proceedings of the 13th EGS Users' Meeting in Japan, Tsukuba, 1-13.; 2006.

27. ICRP. ICRP, 53 . Radiation Dose to Patients from Radiopharmaceuticals. ICRP Publication 53. Ann. ICRP 18 (1-4). Ann ICRP. 1988.
28. ICRP. ICRP, 128. Radiation Dose to Patients from Radiopharmaceuticals: A Compendium of Current Information Related to Frequently Used Substances. ICRP Publication 128. Ann. ICRP 44(2S). Ann ICRP. 2015.
29. ICRP. Radiation dose to patients from radiopharmaceuticals. Addendum 3 to ICRP Publication 53. ICRP Publication 106. Approved by the Commission in October 2007. Ann ICRP. 2008;38(1-2):1-197. doi:10.1016/j.icrp.2008.08.003
30. Boellaard R, Delgado-Bolton R, Oyen WJG, et al. FDG PET/CT: EANM procedure guidelines for tumour imaging: version 2.0. Eur J Nucl Med Mol Imaging. 2015;42(2):328. doi:10.1007/S00259-014-2961-X
31. ICRP. ICRP, 110. Adult Reference Computational Phantoms. ICRP Publication 110. Ann. ICRP 39 (2). Ann ICRP. 2009.
32. ICRP. ICRP, 89. Basic Anatomical and Physiological Data for Use in Radiological Protection Reference Values. ICRP Publication 89. Ann. ICRP 32 (3-4). Ann ICRP. 2002.
33. ICRP. ICRP, 70. Basic Anatomical & Physiological Data for use in Radiological Protection - The Skeleton. ICRP Publication 70. Ann. ICRP 25 (2). Ann ICRP. 1995.
34. Edmond T, Laps A, Case AL, O'Hara N, Abzug JM. Normal Ranges of Upper Extremity Length, Circumference, and Rate of Growth in the Pediatric Population. HAND. 2020;15(5):713-721. doi:10.1177/1558944718824706
35. ICRP. ICRP, 103. The 2007 Recommendations of the International Commission on Radiological Protection. ICRP Publication 103. Ann. ICRP 37 (2-4). Ann ICRP. 2007.
36. Coursey CA, Casalino DD, Remer EM, et al. ACR Appropriateness Criteria® acute onset flank pain-- suspicion of stone disease. Ultrasound Q. 2012;28(3):227-233. doi:10.1097/RUQ.0b013e3182625974
37. Quinn B, Dauer Z, Pandit-Taskar N, Schoder H, Dauer LT. Radiation dosimetry of 18F-FDG PET/CT: incorporating exam-specific parameters in dose estimates. BMC Med Imaging. 2016;16(1):41. doi:10.1186/s12880-016-0143-y
38. UNSCEAR, Report of the United Nations Scientific Committee on the Effects of Atomic Radiation. UNSCEAR. 1993.